Beam Shaping and Control with Nonlinear Optics

Edited by

F. Kajzar

Commissariat a l'Energie Atomique
Gif-sur-Yvette, France

and

R. Reinisch

Institut National Polytechnique de Grenoble
Grenoble, France

KLUWER ACADEMIC PUBLISHERS

NEW YORK, BOSTON, DORDRECHT, LONDON, MOSCOW

eBook ISBN 0-306-47079-9
Print ISBN 0-306-45902-7

Visit Kluwer Online at: http://www.kluweronline.com
and Kluwer's eBookstore at: http://www.ebooks.kluweronline.com

SUB-CYCLE PULSES AND FIELD SOLITONS: NEAR- AND SUB-FEMTOSECOND EM-BUBBLES

A. E. Kaplan, S. F. Straub * and P. L. Shkolnikov

Electrical and Computer Engineering Department
The Johns Hopkins University
Baltimore, MD 21218

ABSTRACT

We demonstrate the feasibility of strong (up to atomic fields) and super-short (few- or even sub-femtosecond) sub-cycle (non-oscillating) electromagnetic solitons -- EM bubbles (EMBs) in a gas of two-level atoms, as well as EMBs and pre-ionization shock waves in classically nonlinear atoms. We show that EMBs can be generated by existing sources of radiation, including sub-picosecond half-cycle pulses and very short laser pulses. We investigate how EMB characteristics are controlled by those of originating pulses. Our most recent results are focused on the related transient phenomena, including EMB formation length, multi-bubble generation and shock-like waves. We also develop the theory of the diffraction-induced transformation of sub-cycle pulses in linear media.

* Also with Abteilung f*ü*r Quantenphysik, Ulm University, Ulm, Germany

1. INTRODUCTION

Contemporary optics usually operates with almost-harmonic, multi-cycle oscillations modulated by an envelope much longer than a single cycle of the oscillations. In fact, any narrow-line radiation is an envelope signal, be it a coherent radiation of a laser, or an incoherent light filtered through a spectroanalyzer. This is also true for any optical pulse, including self-induced transparency (SIT) solitons in two-level systems (TLS) [1], described by Maxwell-Bloch or sine-Gordon equations; mode-locked laser pulses [2] due to multi-mode cavity interaction with laser medium; and optical-fiber solitons [3] due to Kerr-nonlinearity, described by a nonlinear Schrödinger equation [4],etc. To describe any of those pulses, slow-varying envelope approximations are used in both the propagation (by reducing Maxwell equations to a parabolic partial differential equation) and the material response (rotating-wave approximation in constitutive equations). Due to the

Beam Shaping and Control with Nonlinear Optics
Edited by Kajzar and Reinisch, Kluwer Academic Publishers, New York, 2002

availability of very short laser pulses (down to ***~ 6fs*** length [5a] and even below ***5fs*** [5b]), with just a few laser cycles, the efforts are made to improve the envelope approximation at least for linear propagation (see e. g. [6]).

A lot of new experimental techniques and applications, however, such as time-domain spectroscopy [7] of dielectrics, semiconductors and flames [8], and of transient chemical processes, e. g. dissociation and autoionization [9], new principles of imaging [10], and atomic physics by means of photoionization [11], would greatly benefit from the availability of short and intense electromagnetic pulses of ***non–oscillating*** nature, i. e. sub-cycle (almost unipolar) "half-cycle" pulses (HCPs). The spectra of currently available HCPs generated in semiconductors via optical rectification, reach into terahertz domain; these HCPs are ***~400 – 500 fs*** long, with the peak field of ***150 – 200 KV/cm*** [9].

In our recent work [12-14], we have proposed two new different principles of generating much shorter (down to ***0.1 fs = 10^{-16} s***) and stronger (up to ***~ 10^{16} W/cm^2***) pulses. One of these principles is based on stimulated cascade Raman scattering and would result in the generation of an almost periodic train of powerful sub-femtosecond pulses [12], while the other relies on the generation of powerful "EM-bubbles" (EMBs) [13,14], sub-cycle solitary pulses of EM radiation propagating in a gas of two-level or classically nonlinear atoms. The latter effect would allow one to generate a single EMB, or a few EMBs with controllable parameters, each of EMBs propagating with different velocity such that one can easily separate them into individual pulses. In this paper we review our recent research on EM-bubbles and present new related results on transient processes, in particular, on the formation length of EMBs, the generation of multi-EMBs, and the formation of shock and shock-like waves.

Such super-short and intense sub-cycle pulses might be of great interest for the host of applications (see below). Especially significant are non-oscillating ***solitary*** waves that are able to propagate over substantial distances with unchanged shape and length. The exact soliton-like solutions for the nonlinear propagation of unipolar pulses in the strongly-driven two-level system (TLS), described by full Maxwell + full Bloch equations, were found quite a while ago [15]. The solutions have a familiar, ***1/cosh,*** profile, with its duration and velocity related to its amplitude. At that time the authors of Refs. [15] did not believe that these nonlinear pulses were feasible; the main stumbling point they saw was that the pulse intensities would exceed ***~ 10^{14} W/cm^2***, the level unaccessible then. Now optical fields a few orders of magnitude larger are available; however, one of the major problems in the generation of such short (and intense) pulses lies in that the TLS model used in the theory [15] (and in some more recent research [16,17]) will be stretched far beyond its limitations, since intensities above ***~ 10^{14} W/cm^2*** cause very fast over-the-barrier ionization. What are the largest intensities (and thus the shortest lengths) of these pulses that can still be supported by atomic gasses? What are new properties of these pulses beyond the TLS approximation? Fortunately enough, these and other questions about high-intensity super-short pulses, can be addressed using the very fact that the atom is so strongly excited that one can use again its classical (as opposed to quantum) description [13]. In the intermediate domain, a multi-level quantum approach has to be used.

We show here that EMBs are not only feasible but natural for many nonlinear system, both quantum and classical. Their length may range from picoseconds to sub-femtoseconds, depending on their intensity. We call them EM-bubbles to stress their non-envelope nature. We demonstrate that field ionization, a fundamental factor not considered previously, imposes an upper limit on the EMB amplitude and a lower limit on its length; after an EMB reaches its shortest length at some peak amplitude, further increase of the amplitude results in EMB broadening. At some threshold amplitude, the EMB degenerates into a shock wave that is a precursor of a ***dc*** ionizing field -- a new feature which is not present in TLS model. Furthermore, we show that even at much lower peak intensities,

when TLS model may still be valid, the initially smooth HCP may drastically steepen to form a shock-like wave which then breaks in a multi-EMB solution [14]. Unlike a ***dc***-ionization precursor shock wave, this shock-like wave can appear far below the ionization.

EMBs can potentially be as short as ***10 – 0.1 fs,*** with the amplitudes approaching the atomic field. These super-short and intense sub-cycle pulses might be of great interest for the host of applications. They can be used for a "global" spectroscopic technique based on a shock-like excitation across the entire atomic spectrum (to the extent similar to passing atoms through a foil), including normally prohibited transitions. The ionization by a pulse shorter than the orbital period may bridge a gap between conventional photoionization and collisional ionization by a particle [11], with the important difference being that EM pulses offer a control of the quantum state of the atom during the entire process, and hence a control of its final state. This, in turn, has far-reaching implications for applications in time-resolved spectroscopy of transient chemical processes occurring on a femtosecond time scale, e. g. dissociation and autoionization (see e. g. [9]), especially for quantum control of chemical transformations (see e. g. [18]). These new pulses may expand time-domain spectroscopy of dielectrics, semiconductors, and flames [8] from presently available THz domain [7-11] to optical frequencies. One can also envision their applications to probing high-density plasmas, testing the speed of light, imaging molecules and atoms at surfaces, and for an order of magnitude frequency up-conversion due to the large Doppler shift of a counter-propagating coherent light backscattered by EMB, etc. A train of sub-femtosecond pulses with very high repetition rate (~ 125 THz, or with the spacing ***~ 8 fs***), feasible in cascade stimulated Raman scattering [12], can be used for the stroboscopy of atomic motion in a molecule (e. g. during its dissociation).

Another property of EMBs, which may be greatly instrumental in their applications, is their extremely broad spectrum, which ranges ideally from radio-frequencies to visible or even ultra-violet domains. A single pulse of such nature would have a continuous power spectrum from zero frequency to the highest (cutoff) frequency of the pulse,

$$\omega_{cut} \sim 2.6\, t_p^{-1}, \tag{1.1}$$

where t_p is the pulse duration (evaluated at half-intensity). For example, with $\tau = 0.2\,fs$, the cutoff wavelength, $\lambda_{cut} = 2\pi c/\omega_{cut} \sim 2.4\, c\, t_p$, is ***~1440°A*** , i. e. in the far UV. It would be seen by a human eye as an extremely short and powerful ***burst of white light.*** Even the spectrum of a much longer, ***1 fs*** pulse, with $\lambda_{cut} \sim 7200°A$, would still cover the ***infrared, millimeter, microwave, and rf*** domains. Thus the propagation of EMB would be greatly sensitive to a material in which they propagate. The EMB spectrum will be affected strongest by metallic particles or any other good conductors (the part of the spectrum below the respective plasma frequency will be absorbed), or by the presence of water or other substance having strong absorption bands, especially in infrared. Designating the EMB radiation here "S-rays" (where "S" stands for "sub-cycle" or "sub-femtosecond") in analogy to recently demonstrated "T-rays" [10] (THz pulses, see below), we note that the fact that different materials have different transparency for S-rays, suggests a great number of possible applications utilizing EMBs to emulate X-rays without X-ray-induced ionization damage. These S-rays can be used e. g. to monitor processing of high-density computer chips, screening food products at the food-processing facilities, luggage and concealed weapons in the airports, etc. One can also envisage applications of S-rays, similar to T-rays, but in the new frequency domain and with orders of magnitude broader spectra, for medical imaging, in particular, for a new kind of tomography, "S-tomography", with an additional possible advantage of positioning an S-ray source inside a human body. S-rays can also be a useful tool for the diagnostic of high-density fusion plasmas.

This paper is structured as follows. Section 2 discusses a general relationship between the field and polarization, which results in a solitary wave as a solution of full

Maxwell equation + arbitrary constitutive equations. Section 3 addresses an exact EM-bubble solution of full Maxwell+Bloch equation for a two-level system. Section 4 is on EM-bubbles and shock waves which are due to a classical anharmonic potential with ionization. Section 5 discusses various approximate approaches to the transition processes in nonlinear EMB propagation. Section 6 concentrates on EMB generation by half-cycle pulses. Section 7 elaborates on multi-EMB solution; Section 8 discusses shock-like wave fronts due to multi-EMB formation, and Section 9 gives an example of EMB formation by short laser pulse. In Section 10, we develop the theory of diffraction-induced transformation of sub-cycle pulses. In conclusion, we briefly discuss future research on and physical ramifications of EMBs.

2. MAXWELL EQUATIONS AND GENERAL SOLITARY WAVE CONDITION

Maxwell equation for the electric field $\vec{E}$ of a plane EM wave propagating along the z-axis, is:

$$c^2\partial^2\vec{E}/\partial z^2 - \partial^2\vec{E}/\partial t^2 = 4\pi\partial^2\vec{P}/\partial t^2 . \tag{2.1}$$

where $\vec{P}$ is polarization density. Considering a pulse that propagates with a constant velocity, $c\,\beta_{EMB}$, introducing retarded variables, $\tilde{t} \equiv t - z/\beta_{EMB}c$, $\tilde{z} = z$, and imposing a steady-state condition,

$$\partial\vec{E}/\partial\tilde{z} = \partial\vec{P}/\partial\tilde{z} = 0 , \tag{2.2}$$

we reduce Eq. (2.1) to the "solitary wave (EMB) Maxwell equation":

$$\partial^2\vec{E}/\partial\tilde{t}^2 = 4\pi M\,\partial^2\vec{P}/\partial\tilde{t}^2 ; \tag{2.3}$$

where

$$M \equiv \beta_{EMB}^2(1 - \beta_{EMB}^2)^{-1} = const; \tag{2.4}$$

$\sqrt{M}$ is an EMB's normalized relativistic "momentum". Stipulating now that an EMB carries finite energy per unity area of cross-section, i. e. that $\vec{E}, \vec{P} \to 0$ as $|\tilde{z}| \to \infty$(a so called bright soliton condition), and integrating Eq. (2.3) twice, we obtain a universal "EMB-replication" relationship between $\vec{E}$ and $\vec{P}$:

$$\vec{E}(\tilde{t}) = 4\pi M\vec{P}(\tilde{t}) . \tag{2.5}$$

Note that Eq. (2.5) is valid regardless of constitutive relationship between $\vec{P}$and $\vec{E}$. For our further calculations, we assume the field is linearly polarized, so that the wave equation can be reduced to scalar equation, and introduce dimensionless variables: field, f, polarization, p, time, $\tau = t\omega_0$, where ω_0 is a characteristic frequency of the system, and distance, $\tilde{\zeta} = z\omega_0/c$, as well as dimensionless particle density, Q. All these variables and parameters are defined below for quantum and classical models separately; using them, we write Maxwell equation as

$$\partial^2 f/\partial\tilde{\zeta}^2 - \partial^2 f/\partial\tilde{\tau}^2 = Q\partial^2 p/\partial\tilde{\tau}^2 . \tag{2.6}$$

and EMB-replication relationship (2.5) as

$$f(\tilde{\tau}) = QMp(\tilde{\tau}) . \tag{2.7}$$

3. EM-BUBBLES IN TWO-LEVEL SYSTEM

Consider first the pulse propagation in a medium of quantum TLS characterized by the dipole moment, $\vec{d}$, and resonant frequency, ω_0. We introduce normalized variables: the field

$$f \equiv 2\vec{d}\vec{E}/\hbar\omega_0 = 2\Omega_R/\omega_0, \quad with \quad \Omega_R \equiv \vec{d}\vec{E}/\hbar, \tag{3.1}$$

where Ω_R is Rabi frequency; the polarization per atom, $p = \rho_{12} + \rho_{21}$; the population difference per atom, $\eta = \rho_{11} - \rho_{22}$, where ρ_{jk} ($j, k = 1, 2$) are density matrix elements of a TLS (with $\rho_{11} + \rho_{22} = 1$ and $\rho_{12} = \rho_{21}^*$); and time $\tau = (t - z/\beta_{EMB} c)\,\omega_0$, to write full Bloch equations as:

$$\dot{\eta} = -f\dot{p}; \quad \ddot{p} + p = f\eta, \tag{3.2}$$

where the *overdot* designates $\partial/\partial\tau$; we use the notation of [19], which addressed high harmonics generation in a super-dressed TLS. Note that (3.2) is not based on rotating wave approximation. Relaxation is not included in (3.2) since we consider pulses much shorter than TLS relaxation times. The first integral of Eq. (3.2) is square of the Rabi sphere radius,

$$\eta^2 + p^2 + \dot{p}^2 = const = 1. \tag{3.3}$$

The polarization density here is $\vec{P} = N\vec{d}p$ where N is the density of particles; therefore, the parameter Q in (2.6) is as:

$$Q \equiv 4\alpha N\lambda_0 (d/e)^2; \tag{3.4}$$

where e is the electron charge, $\lambda_0 = 2\pi c/\omega_0$ and $\alpha = e^2/\hbar c = 1/137$ is the fine structure constant.

To find an EMB solution for TLS, we substitute the condition (2.7) (with unknown at this point M or β_{EMB}) into (3.2). Having in mind the invariant (3.3) for atoms being initially at equilibrium, $\eta \to 1$ at $|\tau| \to \infty$, such that the first of Eqs. (3.2) gives us $\eta(\tau) = 1 - \dot{f}^2/(2QM)$, we obtain from the second of Eqs. (3.2) a nonlinear equation for the EMB field, $f(\tau)$, as:

$$\ddot{f} - f(QM - 1) + f^3/2 = 0, \tag{3.5}$$

which is a so called Duffing equations. Its first integral is

$$\dot{f}^2 = f^2(QM - 1) - f^4/4 + C, \tag{3.6}$$

(the integration constant $C = 0$ under the bright soliton condition), which determines a separatrix in the phase plane, $\dot{f}$ and f, starting and ending at the point $\dot{f} = f = 0$. The next integration gives us finally an EM bubble, a solitary, non-oscillating wave:

$$f(\tau) = \frac{f_{EMB}}{\cosh(2\tau/\tau_{EMB})}; \tag{3.7}$$

the polarization and population are then:

$$p = f/QM; \quad \eta(\tau) = 1 - fp/2; \tag{3.8}$$

In Eq. (3.7), the amplitude of EMB and its length are respectively:

$$f_{EMB} = 2\sqrt{QM - 1}, \quad \tau_{EMB} = 4/f_{EMB} \tag{3.9}$$

Dimensional EMB amplitude, E_{EMB}, by the definition of f, Eq. (3.1), is

$$E_{EMB} = f_{EMB}\hbar\omega_0/2d = 2\hbar/t_{EMB}d. \tag{3.10}$$

(For EMB length, T, defined at a *half–peak* field, i. e. $T \approx t_{EMB}/1.32 = \tau_{EMB}/1.32\omega_0$, we have $E_{EMB} = 1.32\hbar/Td$.)

Instead of having f_{EMB} as function of M or β_{EMB}, we can express β_{EMB} in terms of f_{EMB}:

$$\beta_{EMB} = \sqrt{M/(1+M)} = [1 + Q/(1 + f_{EMB}^2/4)]^{-1/2} \tag{3.11}$$

or, if $Q \ll 1$ (see below, Section 5),

$$\beta_{EMB} \approx 1 - (Q/2)(1 + f_{EMB}^2/4)^{-1} \tag{3.12}$$

Shorter EMBs have higher amplitudes and move faster, approaching the vacuum speed of light. The lowest allowed speed of a bubble is

$$\beta_{LN} = 1/\sqrt{1+Q} \approx 1 - Q/2. \tag{3.13}$$

which corresponds to a linear propagation of an adiabatically slow pulse.

The Fourier spectrum of EMB,

$$S_f(\omega) \propto 1/\cosh[\pi\omega/2(\Omega_R)_{pk}] \tag{3.14}$$

spreads from zero to the cutoff frequency,

$$\Omega_{cut} \sim (\Omega_R)_{peak} = dE_{EMB}/\hbar. \tag{3.15}$$

Phase-portrait considerations show that with $f = p = 1 - \eta = 0$ at $|\tau| \to \infty$, the ***non–oscillating*** EMB (3.7) is the ***only*** soliton supported by the system. Therefore, surprisingly, regular SIT ***envelope*** solitons [1], which have been obtained in the rotating-wave approximation, are inconsistent with the exact solution (3.7) based on ***full*** Bloch equations (3.2). This indicates that higher-order approximations may render SIT solitons unstable at long enough distances. EMB (3.7) may be regarded as a "full-Bloch" 2π-soliton; by introducing phase (or area)

$$\phi_R(\tau) \equiv \int_{-\infty}^{\tau} f d\tau, \tag{3.16}$$

we get $\phi_R(\infty) = 2\pi$, which points to a "full-Bloch" area theorem.

A similar EMB solution, (3,7), holds also for ***amplifying*** TLS media with the ***inversed*** population, $\eta(|\tau| \to \infty) = -1$. In this case, however [13],

$$\eta = -1 - fp/2, \quad f_{EMB} = (-QM-1)^{1/2}, \quad M < 0, \quad \text{and} \quad \beta_{EMB}^2 > 1. \tag{3.17}$$

Since a TLS with $\eta_\infty = -1$ is a ***non-equilibrium*** system storing pumping energy, β_{EMB} here is ***not*** the speed of energy propagation, so that the fact that $\beta_{EMB}^2 > 1$ (i. e. the EMB moves faster than light) is not incompatible with special relativity. More intense EMBs here move slower, approaching the speed of light from above as their amplitude increases.

4. EM-BUBBLES AND SHOCK WAVES IN A CLASSICAL POTENTIAL

The solution (3.7) is valid within the limitations of our TLS model. In particular, the EMB duration, $t_{EMB} = \tau_{EMB}/\omega_0$, must be shorter that all the atomic relaxation times, which still allows for EMBs as long as $\sim 10^{-9}$ ***s,*** with longer EMBs having lower peak amplitude, Eq. (3.8), and moving slower, Eq. (3.9). It is instructive to consider an example of ***Xe,*** with $\hbar\omega_0 - 8.44eV$, effective dipole size, $d/e \sim 7°A$ (based on the "super-dressed TLS" data for high-harmonic generation in ***Xe*** [19]), and $N \sim 10^{19}$ cm^{-3} ($Q \sim 10^{-2}$). For a ***10ps*** long EMB, we have $E_{pk} \sim 10^3$ ***V/cm.*** Longer pulses can be considered within the TLS model with relaxation. Of a particular interest, however, are the shortest and most intense pulses. When the EMB field approaches the atomic field ($\sim 10^8 - 10^9$ ***V/cm***), the EMB formation is affected mainly by the atomic ionization potential, which limits EMB length and

on EMB within a classical 1-D model of an atom, with a strongly nonlinear potential, $U(x)$, limited at $|x| \to \infty$, to allow for ionization; here x is the electron displacement. Then Bloch equations (3.2) are replaced by a classical normalized equation for the electron motion:

$$\ddot{p} + du(p)/dp = f(\tau). \tag{4.1}$$

with the dimensionless variables and parameters of the system defined as

$$f(\tau) \equiv eE(\tau)x_0/U_0\,; \quad p \equiv x/x_0\,; \quad \omega_0 = \sqrt{U_0/m_e x_0^2}\,; \quad Q = 4\pi N(ex_0)^2/U_0\,; \tag{4.2}$$

where x_0 is an atomic characteristic size, and U_0 is a characteristic energy (e. g., the ionization potential) [20]; m_e is the mass of electron. The polarization density here is $P = Nxe = Nex_0 p$. Note that for EMB, TLS Bloch equations (3.2) reduce to a simple Duffing equation for, e. g. p,

$$\ddot{p} - Ap + Bp^3 = 0, \tag{4.3}$$

with $A = QM - 1$ and $B = (QM)^2/2$, which is equivalent to Eq. (4.1) (with $f = pMQ$) for the simplest classical anharmonic potential,

$$u(p) = p^2/2 + ap^4\,; \quad with \quad a = const > 0. \tag{4.4}$$

Hence, the potential (4.4) can give rise to the same EMB, Eq. (3.7). For an arbitrary potential $u(p)$, the family of EMB solutions, $p(\tau)$, is found from Eq. (4.1) through the quadrature [13]:

$$\int \{MQp^2 - 2[u(p) - u(0)]\}^{-1/2} dp = \pm\tau. \tag{4.5}$$

A "bright" solitary solution to Eq. (4.5) exists, however, only for particular nonlinearities. For example, for (4.4) the nonlinearity must be "positive", $a > 0$ [21]. In general, if u is a smooth, monotonically increasing function of p^2, the "bright" solitary solution exists only if near $p = 0$

$$u(p) - u(0) > p^2 du(0)/d(p^2) \tag{4.6}$$

This requires the atomic potential to have sufficiently "hard walls", which holds for some model potentials [22] (but not for a "soft" potential as e. g. $u = -(1 + p^2)^{-1/2}$ [22]). An example of a model potential that allows for an explicit analytic solution of Eq. (4.5) is:

$$u(p) = p^2(p^2 + b/2)/(1 + p^2)^2 \quad \text{with} \quad b = \text{const} > 0\,. \tag{4.7}$$

To illustrate the limitations imposed by over-the-barrier ionization, consider first a classical "box" potential, $u(p) = 0$ for $|p| < 1$, and $u(p) = 1$ otherwise, in which case the EMB field is

$$f(\tau) = f_{EMB} exp\,(-|\tau|\sqrt{f_{EMB}}), \quad \text{with } f_{\text{EMB}} \le 2, \tag{4.8}$$

and $M = f_{EMB}/Q$. (We presume here that an electron always starts its motion at $p = 0$.) Thus, the maximal field strength, E_{max}, and shortest EMB length, t_{min}, are:

$$E_{max} = U_0/ex_0\,; \quad t_{min} = (x_0/c)\sqrt{m_e c^2/2U_0}\,; \tag{4.9}$$

where U_0 is an ionization limit, and $2x_0$ is the total box width. E_{max} is of the same nature as an atomic field, $E_{at} = E_{max}/2$, i. e. the atom is ionized (in classical terms) by a pulse of a certain shape [here, Eq. (4.8)], if its peak amplitude exceeds E_{max}; t_{min} is the time required for such a field to pull an electron out of the potential well. (With $U_0 = 20eV$ and $x_0 = 1°A$, this results in $E_{max} \approx 2\ 10^9 V/cm$, and $t_{min} \sim 0.4\ 10^{-16}$ s.) To make a connection to atoms with Coulomb long-range attraction, consider now a potential

$$u = 1 - (1 + 2bp^2 + p^4)^{-1/4}. \tag{4.10}$$

with $u - 1 \approx p^{-1}$, at $|p| \to \infty$ It has a single well and satisfies hard-wall condition only when $0 \le b \le b_{cr} = \sqrt{2}/5$. For a given U_0 and atomic number, Z, we have

$$E_{at} = (2/5)^{1/4} U_0/ex_0 ; \tag{4.12}$$

here $r_e = e^2/m_e c^2$ is the classic electron radius. As an illustration, consider a limiting case with $b = 0$. Small-amplitude EMBs are governed again by a Duffing equation, $\ddot{p} - MQp + p^3 \approx 0$, its solitary solution being $p \approx p_{EMB}\sqrt{2}\, sech(\tau p_{EMB})$ (Fig. 1, curve 1).

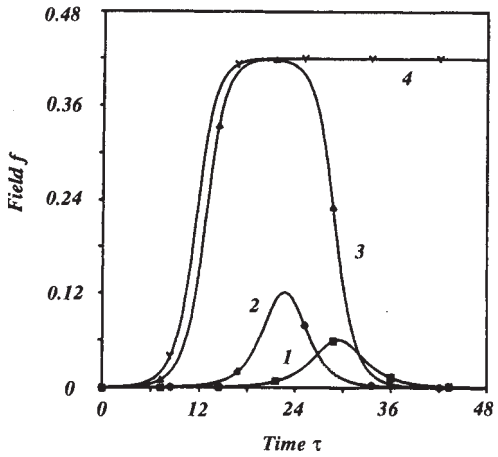

Fig. 1. Normalized field amplitude, f, *vs* time, τ, for steady-state EMB (curves 1-3) and a shock wave (curve 4) due to ionization potential. Curves: 1 -- $MQ = 0.12$, 2 -- $MQ = 0.187$, 3 -- $MQ = (MQ)_{ion} - 10^{-5}$; 4 -- $MQ = (MQ)_{ion} \approx 0.3403$.

Here $p_{EMB} = \sqrt{MQ}$, and therefore, $\beta_{cr} = 0$, i. e. small-amplitude EMBs here can move very slowly, a typical feature of any potential with $du(0)/d(p^2) = 0$. The EMB peak amplitude is $f_{pk} = \sqrt{2(MQ)^3}$. Hence, as its amplitude increases, an EMB moves faster, and shortens. However, at $p_{p\,k} \approx (8/45)^{1/4} \approx 0.65$, $f_{p\,k} \approx 0.122$, EMB length (at the half-peak amplitude) reaches its minimum, $\tau_{A\ min} \approx 5.3$ (at the half-peak amplitude, Fig. 1, curve 2) or $\tau_{I\ min} \approx 2$ (at the half-peak intensity). Assuming $U_0 \approx 24eV$ and $Z = 2$, as in *He*, one obtains the shortest EMB length:

$$t_{I\,min} = 2(r_e Z/c)(m_e c^2/U_0)^{3/2} \sim 10^{-16}\ s . \tag{4.13}$$

(Significantly shorter EMBs can be attained with ionized atoms, e. g. ion beams, which may have ionization potential, U_0, orders of magnitude larger.) As the field amplitude continues to rise, EMB begins to broaden, becoming a flat-top pulse (Fig. 1, curve 3). Finally, at a threshold amplitude, $p_{p\,k} \approx 1.245$, $f_{p\,k} \approx 0.42$, it becomes a shock (anti-shock) wave whose single leading (trailing) edge is a front of an ionizing (de-ionizing) *cw* field (Fig. 1, curve 4) [23]. The amplitude front rises (falls) as $exp(\tau/\tau_{ion})$, with $\tau_{ion} \approx (MQ)^{-1/2} \approx 1.7$. This shock wave is typical to any hard-wall potential with ionization. Our preliminary results indicate, though, that a single-front shock wave becomes unstable, producing a short precursor that travels as a pilot EMB at a faster speed ahead of the group of other, longer and closely spaced EMBs, which merge into a *cd* field far behind the precursor. This pattern persists if one accounts for the plasma due to ionization behind the pilot group of EMBs. In a more detailed picture of a shock wave, the classical over-the-barrier ionization near the threshold must be modified by quantum tunneling.

5. VARIOUS APPROXIMATE APPROACHES TO EMB PROPAGATION

To demonstrate the existence of EMBs (in both quantum and classical eases) most rigorously, we have used so far a "double-full" approach: full Maxwell equation (2.1) + full constitutive equations (3.2) or (4.1) (i. e. without rotating wave approximation). The problem with this "double-full" approach is that at this point we do not have a mathematical theory which would allow us to handle a general solution of the problem (including the case of an arbitrary initial/boundary conditions) with the same degree of confidence and insightfulness as the inverse scattering theory provides for the so called fully integrable partial differential equations, like Kortdeweg-de-Vries, nonlinear Schroedinger, and some other equations. There are no results regarding the full integrability of "double-full" equations, nor even about them being of the same class of equations that can lend themselves to the inverse scattering theory. In physical terms, the very fact that the full nonlinear Maxwell equation allows for the coupling between forward and backward propagating waves, creates a significant complicating factor. Hence, in theoretical consideration of the propagation, as well as in numerical simulations, in particular for all kind of transient problems, we need to look for connections to some better understood equations, at least in certain meaningful limits. Closer consideration shows, fortunately, that "double-full" equations can often be reduced to much simpler equations (with some of them being fully integrable), while keeping them free from a rotating wave approximation and hence open to broad-spectrum solutions.

Our computer simulations have shown that at low density, $Q \ll 1$ (e. g. in gasses, where typically, $Q \sim 10^{-4}$ -10^{-1}), Maxwell equation can be reduced to approximate first-order equation without losing any significant feature of nonlinear propagation. In particular, the EMB solution have the same form, as for full Maxwell equation. This is explained by the fact that when $Q \ll 1$, the propagation velocity approaches the speed of light, $1 - \beta = O(Q)$ $Q \ll 1$. and any retroreflection can be neglected. Assuming now that the wave propagates only in one direction (e. g. positive ζ), using retarded variable $\tau = \tau - \zeta/\beta_{LN}$, and keeping in mind definition (3.13), we transform Maxwell equation (2.6) to the equation:

$$-\frac{\partial^2 f}{\partial \tilde{\zeta}^2} + \frac{2}{\beta_{LN}} \frac{\partial^2 f}{\partial \tilde{\zeta} \partial \tau} = Q \frac{\partial^2 (f - p)}{\partial \tau^2} \tag{5.1}$$

Neglecting in it the term $\partial^2 f/\partial \tilde{\zeta}^2$ (which is small since the pulse changes relatively slow as it propagates along the $\tilde{\zeta}$ axis), and eliminating one derivative, $\partial/\partial\tau$, by integrating the resulting equation over $\partial\tau$, we can write now:

$$\partial f/\partial \tilde{\zeta} = (Q\beta_{LN}/2) \times [\partial (f - p)/\partial \tau]. \tag{5.2}$$

By rescaling the propagation coordinate, $\zeta \equiv \tilde{\zeta} Q \beta_{LN}/2$, we finally obtain:

$$\partial f/\partial \zeta = \partial (f - p)/\partial \tau \tag{5.3}$$

The physical implication here is that nonlinear retroreflection is neglected; the counter-propagating waves are decoupled. The validity of the reduced Maxwell equation can be verified by e. g. using it instead of Eq. (2.6) to obtain EMBs in either quantum and classical limits, as well as by numerical simulations of the transient propagation [14,13]. We have found also that Eq. (5.3) can still be used even if Q is not small, if the field spectrum does not stretch beyond ω_0.

In order to describe the studied process by even simpler equations, and especially by fully integrable ones, one can work now on the simplification of constitutive equations. A major step in this direction is based on the observation that for the most of nonlinear gasses of interest, in particular, for noble gasses, the TLS frequency of the first transition, ω_0, is

extremely high, so that even near-femtosecond pulses and laser oscillations are relatively slow compared with a cycle of that frequency. How slow is "slow" in this case? ***Xe*** has the lowest energy $\mathcal{E}_0 = \hbar\omega_0$ of the first excited level among the noble atoms; with $\mathcal{E}_0 \sim 8.5$ ***ev,*** one cycle of ω_0 is $2\pi/\omega_0 \sim 0.5$***fs.*** For ***He,*** with $\mathcal{E}_0 \sim 20$ ***ev,*** one cycle is ***~ 0.2 fs.*** For any available half-cycle pulses (HCP), the HCP length, t_0, is is three orders of magnitude longer; even the full cycle of e. g. ***Ti:Spph*** laser oscillation is ***~ 2.7 fs*** -- still much longer than $2\pi/\omega_0$ in these gasses. Another important parameter is the dimensionless amplitude of the incident field f_0, (3.1), which is also related to the time scale of the non-linear motion in TLS, $f_0 = O(\tau_{EMB})$. Thus, introducing a parameter, $\varepsilon \equiv \tau_0^{-1} + |f_0|$, we can see that it is very small for HCPs available now or in the foreseeable future. For noble gasses, for example, and with $E_0 \sim 2$ ***MV/cm,*** which is an order of magnitude higher than presently available HCP, we have $f_0 \sim 10^{-2}$; with $t_0 \sim 400$ ***fs,*** we also have $\tau_0^{-1} \sim 10^{-3}$. Hence, if $\varepsilon \ll 1$, we can use a "slow motion" (but no envelopes!) approximation, whereby $f(\tau)$, $p(\tau)$ and $\eta(\tau)$ have their Fourier frequencies much smaller than ω_0. As a first step, "instantaneous weak response", we neglect $\ddot{p}$ in the second of equations (3.2), so that $p_1 = f\eta$, and substitute it in the first of equations (3.2). By integrating it and having in mind the invariant (3.3) (i. e. $\eta = 1$ at $p = \dot{p} = 0$), we obtain

$$\eta_1 = (1 + f^2)^{-1/2}; \quad p_1 = f(1 + f^2)^{-1/2}. \tag{5.4}$$

Writing $p = p_1 + \Delta p$, $\eta = \eta_1 + \Delta\eta$, and neglecting again $\Delta\ddot{p}$ in (3.2), by assuming now that $\ddot{p} \approx \ddot{p}_1$, we obtain in the next approximation: $\Delta p \approx f\Delta\eta - \ddot{p}_1$; $\Delta\dot{\eta} \approx -f\Delta\dot{p}$. This, after evaluating $\Delta\dot{p}$ from the latter equation and substituting it into the former one, results in $\Delta\dot{\eta}(1 + f^2) + ff\eta = f(d^3 p_1/d\tau^3)$, integration of which yields $\Delta\eta \approx (p_1\ddot{p}_1 - \dot{p}_1^2/2)\eta_1$; $\Delta p \approx -p_1\ddot{\eta}_1^2 - p_1\dot{p}_1^2/2$. For $f - p$ we have now:

$$f - p \approx p_1^3\eta_1^{-1}(1 + \eta_1)^{-1} + \ddot{p}_1\eta_1^2 + p_1\dot{p}_1^2/2 \tag{5.5}$$

Two last terms in the rhs of (5.5) reflect the Rabi dynamics, without which EM bubbles would not exist. Rhs of Eq. (5.5) is $O(\varepsilon^3)$; the next approximation correction is $O(\varepsilon^5)$. In the limit $\varepsilon \to 0$, Eq. (5.5) can be further simplified by noticing that since $\eta_1 = 1 - O(\varepsilon^2)$, $\ddot{p}_1 = O(\varepsilon^3)$ as well as $\ddot{p}_1 = \ddot{f} + O(\varepsilon^5)$, and $p_1\dot{p}_1^2 = O(\varepsilon^5)$, we can write, still with the precision $O(\varepsilon^5)$:

$$f - p \approx f^3/2 + \ddot{f}, \tag{5.6}$$

Eqs. (5.3) and (5.6) yield a single self-contained abridged Maxwell-Bloch equation:

$$\partial f/\partial\zeta - (3/2)f^2\partial f/\partial\tau - \partial^3 f/\partial\tau^3 = 0. \tag{5.7}$$

It can be readily shown that solution (3.7) of the full Maxwell-Bloch equations are also solutions of Eq. (5.7). (5.7) is one of the so called Modified Kortdeweg-de Vries (MKdV) equations. The MKdV solutions could be associated [24] with a regular KdV equation, where in the second term, instead of f^2, one has f. MKdV is fully integrable by using inverse scattering method and has an infinite number of invariants [24].

Similar equation can be obtained for a classical anharmonic oscillator (4.1) if the amplitude is not large, i. e. when approximation (4.4) with the coefficient of first-order nonlinearity, a, can be used. In this case, similarly to (5.6), we can write

$$f - p \approx 4af^3 + \ddot{f}, \tag{5.8}$$

and the self-contained wave equation, similar to (5.7), will be again MKdV:

$$\partial f/\partial\zeta - 12af^2\partial f/\partial\tau - \partial^3 f/\partial\tau^3 = 0, \tag{5.9}$$

If the incident field is due to a laser, and is, therefore, oscillating and strong, we may have $\varepsilon \gg 1$. Presuming that TLS model and Bloch equations (3.2) are still valid, the Maxwell-Bloch equations can be reduced to another well-explored equation. Since we

expect the driven polarization, p, to vary rapidly, we can drop p from the second of equations (3.2), assuming that $\ddot{p} \gg p$. Solving (3.2) in this approximation, we readily obtain:

$$\dot{p} = \sin\phi_R ; \quad \eta = \cos\phi_R \tag{5.10}$$

where ϕ_R is Rabi phase (3.16); in this approximation, $\dot{p}^2 + \eta^2 \approx 1$. The reduced Maxwell equation (5.3) can then be written as $\partial f/\partial\zeta \rightarrow \partial f/\partial\tau = \sin\phi_R$, or

$$\partial^2\phi_R/\partial\zeta\partial\tau - \partial^2\phi_R/\partial\tau^2 = \sin\phi_R . \tag{5.11}$$

With a proper choice of retarded coordinate, τ_1, it can be reduced to even simpler equation,

$$\partial^2\phi_R/\partial\zeta\partial\tau_1 = \sin\phi_R . \tag{5.12}$$

These are different forms of so called ***sine–Gordon*** equation, which is fully integrable. It has again the same soliton solution, Eq. (3.7), as general Maxwell+Bloch equations do. While using Eqs. (5.10)-(5.12), one has to be cautious about choosing boundary conditions; only those functions $f(\tau)$ at $\zeta = 0$ that satisfy a condition on the area of the pulse (see below), $S \equiv \phi_R(\infty) = 2\pi n$, where n is integer, are applicable for simulations. (The best choice would be $S = 0$, since it would allow one to vary the amplitude of the incident field once the shape of the field is chosen). If S is not integer of 2π, this approximation will be inconsistent with the physics in the sense that it may happen that neither area $S(\zeta)$ of the propagating pulse nor its energy W are invariants. Fortunately, the condition $S = 0$ can easily be satisfied for an oscillating field, which is exactly the area of the intended applicability of (5.10)-(5.12). However, even more stringent conditions may be imposed by the fact that TLS model is invalid when the Rabi frequency, Ω_R, exceeds the TLS frequency, ω_0, i. e. when $f >> 1$. Some other approximations that result in fully integrable equations can be found in [15-17].

We have to note that at this point no mathematical proof exists that in the general, "double-full" formulation, EMBs are real solitons in the sense of full integrability of the full Maxwell + full constitutive equations, and that, therefore, EMBs are absolutely stable. Our numerical simulations for both TLS and nonlinear classical potentials show that small EMB due to reduced Maxwell equation (5.3) are stable against both small and large (e. g. collision with another EMB) perturbations, which is consistent with the results of Ref. [15] for TLS. Large EMBs (approaching the ionization threshold) may become unstable and break down into smaller EMBs. In a related simulation, we have discovered that significantly below the ionization threshold the EMBs are remarkably stable upon temporal or spatial changes of medium parameters. In particular, when the gas density, N, was changed by two orders of magnitude along the path of propagation, the EMB profile and its length remained stable; only its velocity, β_{EMB}, was adjusting to a varying density, such that

$$N(z)\, M(\beta_{EMB}) = inv . \tag{5.13}$$

An EMB generated e. g. in a gas jet can therefore "slide" into vacuum without distortion.

Finally, it is worth noting that a very interesting recent work [25] suggested generation of non-oscillating or unipolar EM solitons and shock-like waves in nonlinear dielectrics due to collective effect (phonons) in a crystal lattice. The time scale of these solutions is much larger than those discussed here, with the soliton length t_p being much longer than a cycle of the transverse optic lattice resonant frequency, ω_{OT}, i. e. $t_p \ll \omega_{OT}^{-1}$; t_p would be no shorter than a few picoseconds for the best of materials. The nonlinearity in [25] scales as E^2, with the single soliton having the profile of $\cosh^{-2}$; the important fact is that, as shown in [25], the ***full*** nonlinear Maxwell equation for the case in consideration (based on simplified constitutive equation that uses the assumption of low frequencies and relatively weak field) can be reduced to a fully integrable Boussinesq-like equation.

6. EM-BUBBLE GENERATION BY HALF-CYCLE PULSES

One of the major avenues of EMB-generation [13] is to use existing half-cycle pulses (HCPs) [7-11] to launch much shorter EMB pulses in a nonlinear medium via a transient propagation process. At first, it is important to obtain ***50 fs*** to ***~ 5 fs*** long EMBs, thus attaining one to two orders of magnitude enhancement over available HCPs. In our computer simulations [13,14], we found that distinct individual EMBs could be obtained with a HCPs. In these simulations, we used incident HCPs (i. e. the solution $f(\zeta,\tau)$ at $\zeta = 0$) of ***various*** profiles resembling a typical experimental profile, in particular, Gaussian,

$$f(\tau) \propto exp[-(2\tau/\tau_0)^2] \tag{6.1}$$

and ***1/cosh*** profile, i. e. the same as EMB, (3.7), but with its amplitude, f_0, unrelated to its length, τ_0:

$$f(\tau) = f_0/cosh(2\tau/\tau_0) \tag{6.2}$$

All of them show very similar behavior in the formation of EMBs; in this paper we will address ***1/cosh*** profile (6.2) as the only one that can bring up exact analytical results related to the formation of ***multiple*** EMBs; however, most of our results here on the parameters of the leading (i. e. largest and fastest) EMB, "EMB-precursor", in particular its amplitude, length, and formation distance, will be valid for any incident HCP. The TLS approximation is valid with great margin, if the instantaneous Rabi frequency is relatively small, $f << 1$, which, as was shown in the previous section, is the case for the available HCPs; for instance, in noble gasses, even with still unavailable $E = 2$ MV/cm, $f \sim 10^{-2}$.

For a given length of the incident HCP, τ_0, HCP's threshold (minimal) amplitude required to attain a single EMB, provided the HCP has a profile (6.2), according to (3.9) and (3.10), is:

$$f_{thr} = 4/\tau_0, \quad or \quad E_{thr} = 2\hbar/t_0 d. \tag{6.3}$$

In most of our runs, we used $\tau_0 = 4000$, which corresponds to $t_0 \sim 313$ fs (or 413 fs at pulse's half-amplitude), for Xe ($\hbar\omega_0 \approx 8.5$ eV; $d/e \approx 7$ Å [13,14]); in this case, $f_{thr} = 10^{-3}$ and $E_{thr} \approx 60$ KV/cm.

Typical patterns of EMB formation are shown in Figs. 2 and 3.

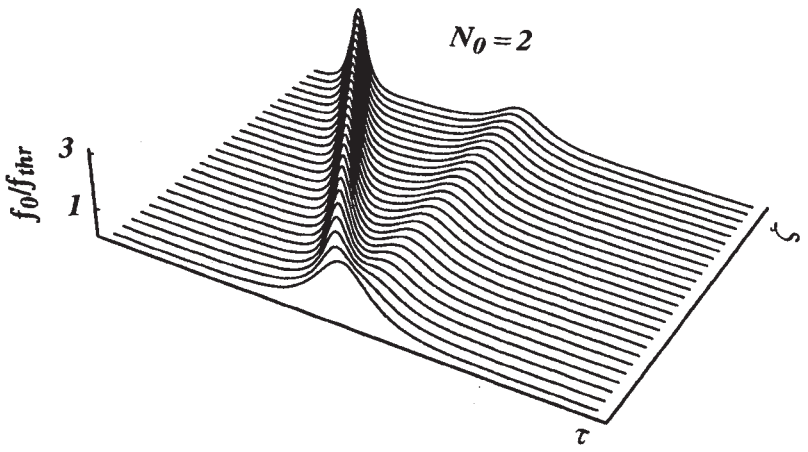

Fig. 2. Double-EMB formation by HCP with $f_0 = 2f_{thr}$.

Fig. 2 depicts a double-EMB formation for $f_0 = 2f_{thr}$; the larger EMB here is $3f_{thr} = (3/2)f_0 \rightarrow 180$ KV/cm, and of the weaker one, f_{thr}; they are respectively 104 fs and 313 fs long. Fig. 2 can also be seen as a collision of two EMBs, with each of them coming out unaffected by the collision (aside from slight shift of their center lines of propagation); this can be shown by retracting the plot back in $\zeta < 0$. For larger f_0, more EMBs are formed and the strongest EMB moves faster than the rest of the pack, leading the train as a precursor. The "density plot" showing the linear trails of individual EMBs moving with different velocities, with the front trail being due to EMB-precursor, is depicted in Fig. 4. As f_0 increases, the precursor is growing stronger and shorter, and the distance, ζ_{EMB}, for it to break away from the mother-HCP, is decreasing. Fig. 3 depicts multi-EMB formation for $E_0 = 2$ MV/cm ($f_0 \approx 3.3 \times 10^{-2} = 33 f_{thr}$), expected to be available in the near future. In this case, z_{EMB} is estimated (see end of Section 8) from $\zeta_{EMB} \sim 1.23 \times 10^5$; for Xe at 10 atm ($Q \sim 0.57$), it translates into $z_{EMB} \sim 12.5$ cm. The precursor here is 4.8 fs long, two orders of magnitude shorter than available HCPs.

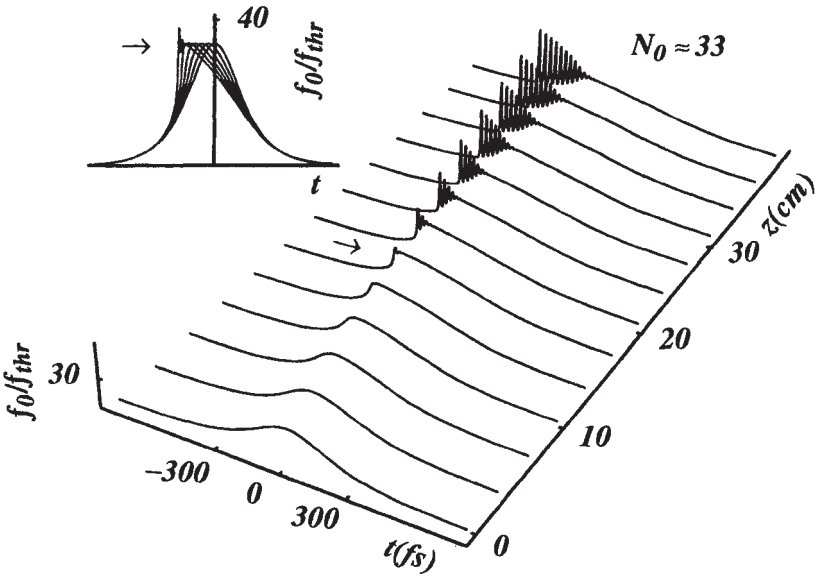

Fig. 3. The formation of multi-EMBs and a shock-like wave front for $f_0 f_{thr}^{-1} \approx 33$ as the wave propagates in ζ; inset: superimposition of the field profiles at different ζ illustrating the front formation.

Experiment- and application-wise, it is important to know how the properties of EMBs are controlled by the incident HCP. In this respect, one has to answer a few important questions: given the amplitude, E_0, and length, t_0, of the incident HCP, (i) what are the leading EMB's amplitude and (ii) its length? (iii) how many EMBs (per one HCP) can be

generated? (iv) what are amplitudes and lengths of these EMBs? and (v) what is the formation distance for the first EMB? Although the equations governing the wave propagation are fully integrable in certain approximations (see the preceding section), the above questions cannot in general be answered analytically. Our combined numerical and analytical efforts [14] allowed us, however, to obtain remarkably simple results, which could be summarized as follows: the amplitude of EMB, E_{EMB}, is proportional to (and larger than) the amplitude E_0 of an incident HCP; the EMB's length is inversely proportional to E_{EMB}; the number of the EMBs is proportional to the area of the incident HCP. We have also discovered that when multiple EMBs are generated, they form at some point a shock-like wave front, its its formation being is proportional to E_0^{-2}. We have shown that the distance of the first EMB formation is proportional to E_0^{-3} if E_0 is relatively small; for sufficiently large E_0, this process coincides with the shock-like wave formation. The main good news is that very short EMBs can be generated by a long HCP with sufficiently large amplitude.

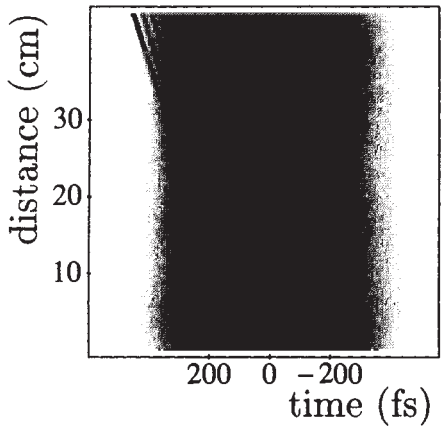

Fig. 4. Density plot for the propagation shown in Fig. 3; note that the "trails" of individual EMBs make straight lines, i. e. each one of them propagate with its individual constant velocity, β_{EMB}, (3.11).

In our computer simulations [14], using HCPs of ***various*** profiles [in particular, Gaussian (6.1), and $cosh^{-1}$ (6.2)], we found that an EMB-precursor shows a linear dependence of its amplitude, f_{EMB}, on the incident amplitude, f_0, regardless of the profile:

$$f_{EMB} \approx af_0 - (a-1)f_{thr}, \quad with\ a = const \sim 2. \tag{6.4}$$

For the profile (6.2), Eq. (6.4) becomes exact with $a = 2$, so that

$$f_{EMB} = 2f_0 - f_{thr}, \tag{6.5}$$

see Fig. (5). This also gives the precursor's length:

$$\tau_{EMB} \approx 4 / (2f_0 - f_{thr}) \simeq 2\tau_0 / (\tau_0 f_0 - 2). \tag{6.6}$$

Due to (6.5) and (6.6), the amplitude and length of the largest EMB tend to constants as the HCP's length τ_0 increases (Fig. 6). Hence, to attain large and short EMB, there is no need to use a short incident pulse; the only prerequisite is a sufficiently high amplitude.

To explain these results and to find other characteristics of the EMBs, in particular their formation distance, we use here the approach reminiscent of that developed in the theory of modulation instability in self-focusing and in propagation of pulses in nonlinear optical fibers. Approximating an initially long and smooth HCP by an almost ***dc*** wave with the amplitude of the incident slow pulse, and evaluating the propagation characteristics of this wave, we analyze the behavior of small ***perturbations*** of this wave.

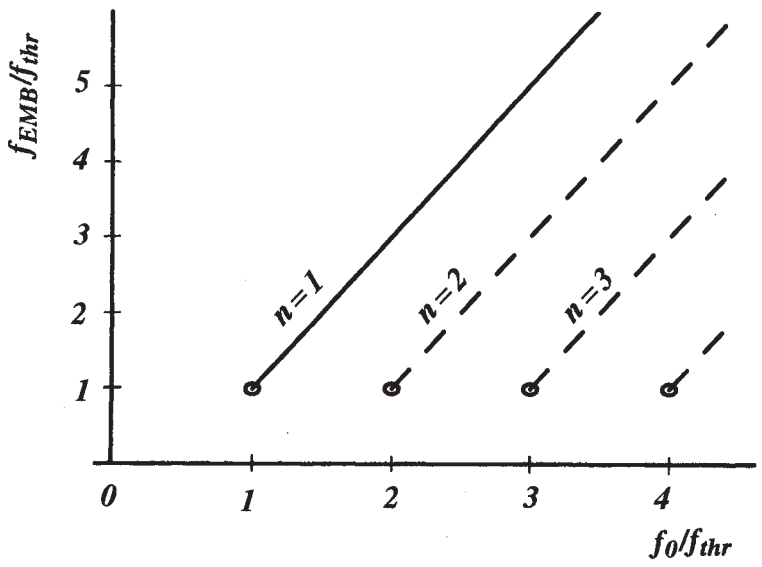

Fig. 5. The EMB's amplitude, f_{EMB}, *vs* the amplitude, f_0, of the incident HCP (both normalized to f_{thr}). Curves: solid -- EMB-precursor; broken -- higher order EMBs.

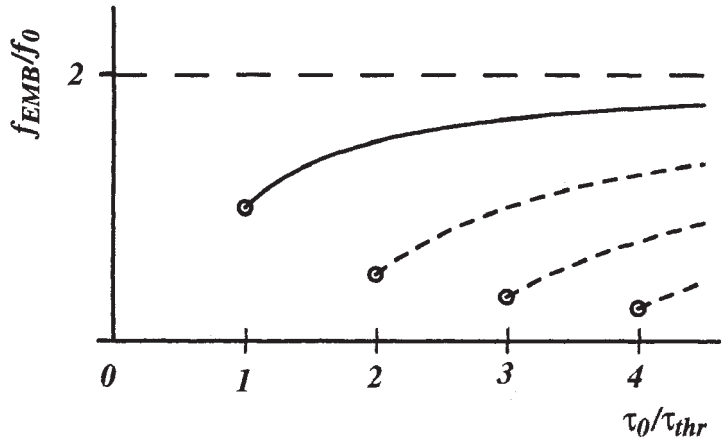

Fig. 6. The EMB's amplitude, f_{EMB}, *vs* the length, τ_0, of the incident HCP (normalized to f_{thr} and τ_{thr}, respectively). Curves: solid -- EMB-precursor; broken -- higher order EMBs.

Linearizing the original equations with respect to these perturbations, and deriving a dispersion equation for their spectral components, we find then the spectral component with the fastest phase change. The speed of propagation of this unique component, its frequency, as well as a spatial scale (the shortest of all the components) at which a sufficient phase accumulation occurs, -- all this point to an EMB-precursor that will develop from this component.

Note that this approach allows us to still work with full Maxwell+constitutive equations; to demonstrate it, we show here how the meaningful results can be obtained for ***full*** Maxwell+Bloch equations (2.6) and (3.2); we will also keep track of simplifications stemming from reduced equations (5.3) and (5.6), (5.7). Assuming a field with the amplitude $f_0 = const$ in Eqs. (2.6) and (3.2), one obtains that the population difference, polarization per atom, "momentum" parameter, and the speed of this "***dc***" field are respectively:

$$\eta_0 = \Omega_{ST}^{-1}; \quad p_0 = f_0\Omega_{ST}^{-1}, \quad QM_0 = \Omega_{ST}, \quad \text{and} \quad \beta_0 = (1 + Q\Omega_{ST}^{-1})^{-1/2}, \tag{6.7}$$

where

$$\Omega_{ST} \equiv (1 + f_0^2)^{1/2} \tag{6.8}$$

is the Stark-shifted frequency of TLS due to the field effect. Solving now (2.6) and (3.2) for small perturbations of this solution, and representing these perturbations in terms of spectral components, $exp[i(q\tilde{\zeta} - \Omega\tau)]$, we obtain the dispersion relationship between the wave number of the perturbation component q and its frequency Ω:

$$q = \Omega \sqrt{1 + Q/\Omega_{ST}(\Omega_{ST}^2 - \Omega^2)} \tag{6.9}$$

In the linear ($f_0 \to 0$), low frequency ($\Omega \to 0$) limit we have:

$$q_{LN} = \Omega\ (1 + Q)^{1/2}. \tag{6.10}$$

The part of q which is due to both the nonlinearity and dispersion if $Q << 1$ is thus:

$$\Delta q \equiv q - q_{LN} \approx (Q\Omega/2)[\ \Omega_{ST}(\Omega_{ST}^2 - \Omega^{2)-1} - 1\ ] \tag{6.11}$$

The lowest $\Delta q(\Omega) < 0$ corresponds to the fastest perturbation. Looking for the minimum of Δq, we obtain the frequency, $\Omega = \Omega_{fast}$, of this component as:

$$(\Omega_{fast}/\Omega_{ST})^2 = (2\Omega_{ST}^3 + 1 - \sqrt{8\Omega_{ST}^3 + 1}\ )/2\Omega_{ST}^3; \tag{6.12}$$

hence if $f_0^2 \ll 1$, we have

$$\Omega_{fast} \approx f_0^2/2. \tag{6.13}$$

Substituting $\Omega = \Omega_{fast}$ into (6.9), we evaluate q_{fast} and the phase velocity $\beta_{fast} \equiv \Omega_{fast}/q_{fast}$, of this component in the case $Q << 1$ as:

$$\beta_{fast} \approx 1 - Q/(1 + \sqrt{8\Omega_{ST}^3 + 1}\ ) \tag{6.14}$$

Comparison with (3.11) shows that a matching EMB, $\beta_{EMB} = \beta_{fast}$, has an amplitude:

$$f_{fast} = [2(\sqrt{8\Omega_{ST}^3 + 1}\ - 3)]^{1/2}. \tag{6.15}$$

or, for $f_0^2 \ll 1$ [14],

$$f_{fast} \approx 2f_0 \tag{6.16}$$

Eq. (6.16) confirms the linear dependence between f_0 and f_{fast} in (6.4) and fits perfectly the coefficient $a = 2$ in (6.5). Note that in an ideal dc field, $\tau_0 \to \infty$ and thus $f_{thr} \to 0$, which explains the difference between (6.5) and (6.16).

The same approach can be used to estimate the precursor formation distance, $\tilde{\zeta}_{EMB}$, but only in the limited range of the parameters, since in general $\tilde{\zeta}_{EMB}$ depends on total area of HCP (see below). To still use perturbation approach, we substitute again $\Omega = \Omega_{fast}$ into

(6.9) and estimate ζ_{EMB} as a distance at which a certain change of phase, $\phi = 0(2\pi)$, is accumulated (the best fit is provided by $\phi = \pi\sqrt{10}$). In particular, if $f_0 << 1$, $\Delta q_{fast} \approx -Qf_0^3/\sqrt{2}$, and [14]

$$\tilde{\zeta}_{EMB} \sim \pi\sqrt{10}\,|\,\Delta q_{fast}\,|^{-1} = 2\pi\sqrt{5}\,Q^{-1}f_0^{-3} \quad or \quad \zeta_{EMB} \sim \pi\sqrt{5}f_0^{-3}\,. \tag{6.17}$$

(curve 1 in Fig. 7). Thus, ζ_{EMB}, estimated by a phase change, scales as f_0^{-3}. This compares well with the distance of first appearance of a saddle point, $\partial f/\partial\tau = \partial^2 f/\partial\tau^2 = 0$ (dots in Fig. 7), in the numerically obtained field profile up to $(f_0/f_{thr})_{cr} = N_{cr} \sim 4$.

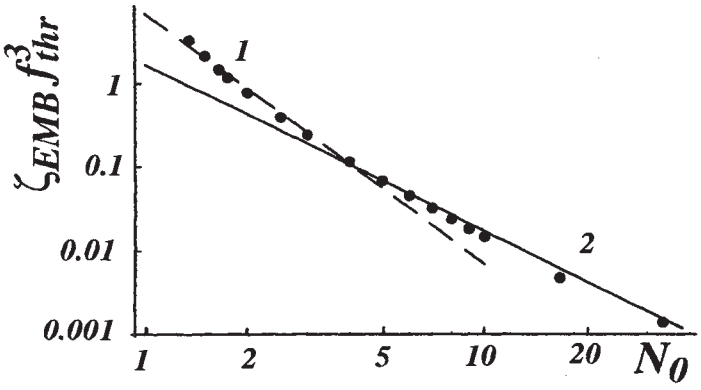

Fig. 7. The normalized formation distance, $\zeta_{EMB} f_{thr}^3$, of EMB-precursor *vs* normalized incident amplitude, $N_0 = f_0 f_{thr}^{-1}$. Curves: 1 -- $\pi\sqrt{5}\,N_0^{-3}$, (6.17), 2 -- $\sqrt{3}\,N_0^{-2}$, (6.18); dots -- first saddle point appearance in a field profile.

For larger f_0, when multiple EMBs are generated (see below), right before the EMB-precursor breaks away, the initially smooth HCP drastically steepens to form a shock-like wave (Fig. 3), which, unlike a *dc*-ionization shock wave (section 4), can appear now far below ionization. Its formation distance, ζ_{sh} (curve 2 in Fig. 7), that can be analytically calculated based on the theory of shock-like wave, section 8 below, is as [14]:

$$\zeta_{sh} \approx \zeta_{EMB} \approx \sqrt{3}\,(f_0^2 f_{thr})^{-1}\,; \quad (f_0 > 4f_{thr})\,, \tag{6.18}$$

which scales as f_0^{-2} now.

7. MULTI-BUBBLE SOLUTION

When the incident amplitude of HCP, f_0, sufficiently exceeds the threshold of EMB formation, f_{thr}, more than one EMB will be generated, as one can see from Figs. 2 and 3. In the limit $f_0 << 1$, when the propagation is described by modified KdV (5.7), one can develop the analytical theory on N-bubble solutions for the profile (6.2). The results of our theory, to be published elsewhere, are based on invariants of MKdV [24], and are briefly summarized here. Total number of EMBs, N_{EMB}, is:

$$N_{EMB} = L(N_0), \quad with \quad N_0 \equiv f_0 f_{thr}^{-1} = f_0 \tau_0 / 4, \tag{7.1}$$

where $L(x)$ the largest integer not greater than x. For $N_0 >> 1$, N_{EMB} is proportional to the incident HCP area, $f_0 \tau_0$, With the EMB-precursor designated by number 1, the amplitude, f_n of the n-th EMB is given by an amazingly simple formula:

$$f_n f_{thr}^{-1} = 2(N_0 - n) + 1, \quad n \le N_0, \tag{7.2}$$

such that the decrement,

(7.3)

is independent of n. Since each bubble with the amplitude f_{EMB} carries an energy:

$$W_{EMB} = f_{EMB}^2 \quad \tau_{EMB} = 4 f_{EMB}, \tag{7.4}$$

which is proportional to its amplitude, f_{EMB}, a unique quality of the function (6.2) is that the energies of the bubbles generated by it, are ***equidistant,*** or quantized, in the way reminiscent of the energy spectrum of a linear oscillator, with the "quantum" (or "quton") of their energy spectrum being $\Delta W_q = 2 W_{thr}$. It is worth noticing that when N_0 is an integer, the lowest energy of a bubble is exactly $W_{thr} = \Delta W_q / 2$, which again is reminiscent of the energy of the ground level of a linear oscillator, being equal to half the quantum of excitation.

For the EMB-precursor, $n = 1$, Eq. (7.2) coincides with Eq. (6.5), as expected. If f_0 is an integer of f_{thr} (6.3), the incident HCP gives rise to an ***exact*** **N**-bubble solution. Otherwise, a part, ΔW_{rad}, of its incident energy, W_0, is radiated away into non-trapped modes; their relative impact decreases rapidly as the total number of EMBs increases:

$$\Delta W_{rad} W_{thr}^{-1} \equiv [N_0 - L(N_0)]^2 \le 1. \tag{7.5}$$

Thus ΔW_{rad} is always smaller than the critical (smallest) energy, W_{thr} of a bubble (for the fixed τ_0). Furthermore, as the incident amplitude increases, the relative maximum energy of un-trapped radiation greatly decreases:

$$\Delta W_{rad} W_0^{-1} \le N_0^{-2}. \tag{7.6}$$

8. SHOCK-LIKE WAVE FRONTS

When the incident HC-pulse is sufficiently strong to generate many EMBs ($N_0 >> 1$), right before the EMB-precursor is formed, the initially smooth HCP drastically steepens and forms a shock wave at the front of the pulse. The formation of the EMB-precursor coincides with the point in space at which the shock wave is steepest; this front is about τ_{EMB} long. After this point, the shock wave breaks into the train of EMBs. To investigate this shock wave formation and estimate the location of the breaking point, we make further approximation, which may be called "instantaneous reaction", by dropping the higher derivative terms in the constitutive equations of the system. In the limit $Q << 1$, Eq. (5.3) is replaced in the case of TLS by

$$\partial f / \partial \zeta = [1 - (1 + f^2)^{-3/2}] \partial f / \partial \tau, \tag{8.1}$$

and in the case of the anharmonic classical oscillator (5.3) -- by

$$\frac{\partial p}{\partial \tau} = \left(\frac{\partial}{\partial \zeta} - \frac{\partial}{\partial \tau} \right) \left(\frac{du}{dp} \right) \tag{8.2}$$

If the HCP amplitude is small, $f << 1$, Eqs. (8.1) and (8.2) are further simplified to

$$\partial f/\partial\zeta = 12af^2\,\partial f/\partial\tau; \tag{8.3}$$

with a being the same as in Eq. (4.4) for classical anharmonic potential; $a = 1/8$ for TLS. Any equation in the form

$$\partial f/\partial\zeta = F(f)\partial f/\partial\tau, \tag{8.4}$$

where $F(f)$ is some smooth function, has a general solution whereby each point of the solution, $f = f_1$, moves with the fixed velocity determined by f_1:

$$f[\tau + F(f_1)\zeta] = f_1. \tag{8.5}$$

where in the case of Eq. (8.1), $F(f) = 1 - (1+f^2)^{-3/2}$, and of Eq. (8.3), -- $F(f) = 12af^2$. Evaluating now the derivative $\partial f/\partial\tau$ at a point ζ, we find

$$\frac{\partial f}{\partial\tau} = \frac{(\partial f/\partial\tau)_{\zeta=0}}{1 + \zeta(dF/df)(\partial f/\partial\tau)_{\zeta=0}} = \frac{(\partial f/\partial\tau)_{\zeta=0}}{1 + \zeta(\partial F/\partial\tau)_{\zeta=0}} \tag{8.6}$$

such that for any nonzero $(dF/df)(\partial f/\partial\tau)_{\zeta=0}$, there will be a point ζ, at which $\partial f/\partial\tau \to \infty$, which signifies the formation of shock wave. Since the formation of the shock wave will be arrested at the amplitude f_1, at which $(\partial F/\partial\tau)_{\zeta=0}$ is maximal, we find that for the profile (6.2), such a point is at $cosh^2(2\tau/\tau_0) = 3/2$, or at $f = f_0\sqrt{2/3}$, with $[(\partial F/\partial\tau)_{\zeta=0}]_{max} = -32af_0^2(\tau_0\sqrt{3})^{-1}$. Hence the distance of formation of the shock wave is

$$\zeta_{sh} = -\frac{1}{[(\partial F/\partial\tau)_{\zeta=0}]_{max}} = \frac{\tau_0\sqrt{3}}{32af_0^2}, \tag{8.7}$$

which in the case of TLS (i. e. when $a = 1/8$ and $\tau_0 = 4/f_{thr}$) gives Eq. (6.18). At the point of shock wave formation, the full constitutive equation will prevent the discontinuity of the exact solution, and break the shock wave into the train of solitons; the length of the steepest rise of the shock wave is thus determined by the EMB-precursor time, (3.9).

Consider an example, $E_0 = 2$ *MV/cm* with $t_0 \sim 313$ *fs* (or *413 fs* at pulse's half-amplitude), in *Xe.* In this case $f_{thr} = 10^{-3}$ and $E_{thr} \approx 60$ *KV/cm* ($f_0 \approx 3.3 \times 10^{-2} = 33f_{thr}$), and the formation distance is estimated, Eq. (6.18), as $\zeta_{EMB} \sim 1.54 \times 10^6$, which under *10 atm* pressure ($Q \sim 0.57$) translates into $z_{sh} \sim 12.5$ *cm.* The EMB-precursor here is *4.8 fs* long, two orders of magnitude shorter than available HCPs. Note that in all these examples with HCPs, the field $f << 1$ ($\Omega_R << \omega_0$) is much below the super-dressed regime of TLS, and therefore far from the ionization. The distance of the shock wave (and first EMB) formation can be shortened, if its leading front is sharpened (e. g. by a shatter), such that $\tau_{lead} < \tau_0$. The distance ζ_{sh} can then be evaluated by multiplying (8.7) by a factor τ_{lead}/τ_0; in the above example, if the HCP leading front is shortened down to ~ *40 fs,* the shock formation distance reduces to ~ *1.25 cm.*

9. EM-bubbles generation by a short laser pulse

Even the highest realistically expected fields of HCPs are still much lower that the amplitudes readily attainable in lasers. The possibility of the EMB formation in ***each*** laser cycle, therefore, increases tremendously, although the ensuing picture becomes more complicated due to the multiple EMB interactions, when the regular laser radiation with many oscillations in the envelope is used instead of HCPs. Indeed, since the laser cycle is much shorter (e. g., the cycle duration for the radiation with $\lambda = 0.9\ \mu m$ is ~ *3 fs*), with the laser intensities of ~ 10^{14} *W/cm*^{2} (which corresponds to the field ~ 2.7×10^8 *V/cm*), the EMB formation distance reduces to less than *1 mm,* and the EMB becomes an order of magnitude shorter than the optical cycle. Fig. 8 shows a group of EMBs developing from a very short (*6 fs*) laser ***pulse*** with the relatively low peak intensity 6.8×10^{12} *W/cm*^{2}. One can see that

the EMB formation length is about ***0.1 – 0.2 mm,*** and the length of the EMB-precursor is about ***0.5 fs.*** There is a distinct possibility that the very high-order harmonics generation [26] in noble gasses might be to a substantial degree attributed to the multiple EMB formation, which would explain many major features of the HHG phenomenon, such as its puzzling insensitivity to the phase mismatch at different high harmonics, broadening and shift of harmonic spectra, etc.

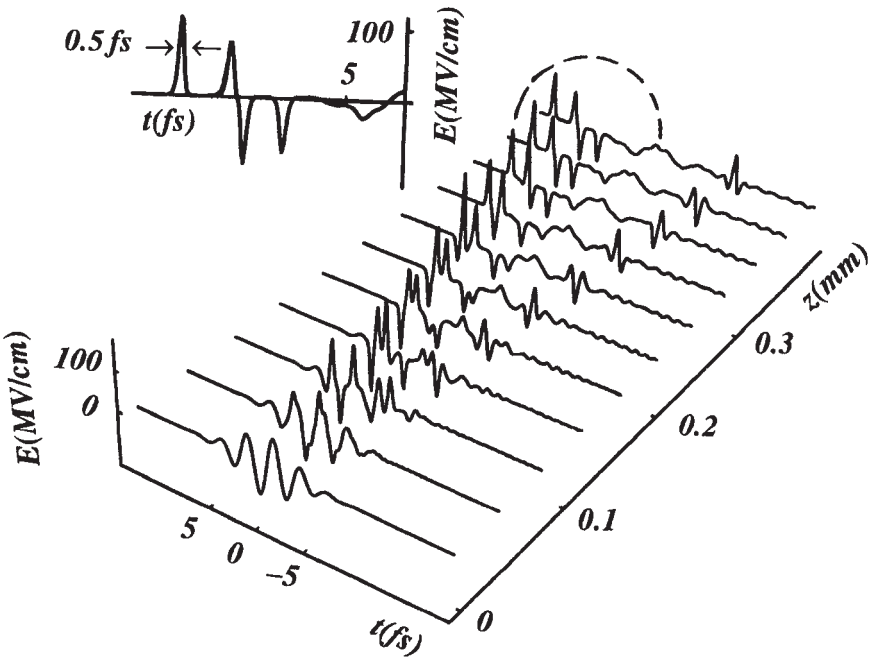

Fig. 8. EMB formation from an oscillating laser pulse ($t_p \approx 6$ *fs*). Inset -- a final cross-section magnified to show EMBs.

10. DIFFRACTION-INDUCED TRANSFORMATION OF SUB-CYCLE PULSES [27]

So far we were focusing on nonlinear propagation of sub-cycle pulses, being mostly interested in formation of solitons and EM-bubbles in nonlinear media. >From the application point of view it is important also to know what would happen with a sub-cycle pulse when it is emitted into a linear medium (e. g. air or vacuum). It is clear that the diffraction will immediately affect not only spatial profile of the pulse, but also its temporary profile, since different Fourier components of such a broad-band pulse diffract differently. Low-frequency components diffract most drastically, almost as the radiation of a point source, while very high-frequency components may propagate almost without diffraction like geometro-optical rays. Thus, on-axis radiation will be loosing the low-frequency part of its

spectrum, while the off-axis radiation will be loosing its high-frequency part, which will result in a peculiar transformation of both of them. In particular, we show below that the on-axis pulse in the far field area will be mimicking the time-derivative of the original pulse (thus formating "full-cycle" pulse out of half-cycle pulse), while in addition to that, the off-axis propagation also results in the lengthening of this pulse.

In this Section, following our recent work [27], we develop an analytic approach to the theory of ***linear*** diffraction transformation of pulses with super-broad spectra and arbitrary time dependence, in particular half-cycle (unipolar) pulses. Since this theory has much broader applications than nonlinear processes, we will develop it for spatially 3D case (or precisely speaking, 2+1+1D case, i. e. with the spatial cross-section of the beam having two dimensions, and other two dimensions formed by the axis of propagation and time). We found close-form solutions for pulses with initially Gaussian spatial profiles having either $\cosh^{-1}$-like or Gaussian time dependence. The far-field propagation demonstrates time-derivative behavior regardless of initial spatio-temporal profile.

Diffraction is one of the fundamental manifestations of the wave nature of light. The diffraction theory of monochromatic light has been developed in great details (see e. g. [28]). In general this theory is heavily loaded with various special functions, but the development of lasers advanced the use of Gaussian beams, which are auto-model solutions of a so called paraxial approximation (PA) and allow one to handle the diffraction of spatially-smooth optical beams in a very simple way (see e. g. [29]).

Recent developments [7-11,18] in optics resulted in the generation of short and intense EM pulses of ***non–oscillatory*** nature, or almost unipolar "half-cycle" pulses (HCPs), with extremely broad spectra that start at zero frequency; even existing pulses have many exciting applications (see introductory section and Refs. [7-11,18]). The spectra of currently available HCPs generated in semiconductors via optical rectification, reach into terahertz domain; they are ***~400–500 fs*** wide, with the peak field up to ***150–200 KV/cm.*** In our recent work part of which is described in this paper (see also Refs. [12-14]), we proposed new different principles of generating much shorter (down to $0.1\ fs = 10^{-16}\ s$) and stronger (up to $\sim 10^{16}\ W/cm^2$) HCPs. As it was pointed out above, different frequency components in HCPs diffract differently, far away from the source HCPs propagate with significant dispersion and distortion even in free space [7-11,18,30,31]. This phenomenon calls for the diffraction/transformation theory of pulses with super-broad spectra, preferably comparable in its simplicity and insights with that of Gaussian beam diffraction of monochromatic light. Such a theory could also apply to other fields of wave physics: acoustics, solid-state physics and quantum mechanics.

The work [31] analyzed asymptotic field behavior in far-field area of a beam with an (initially) Gaussian spatial profile and found time-derivative behavior in that area. Ref. [31] considered only the fields with an also (initially) Gaussian ***temporal*** profile. However, even for that profile, no global analytic solution (even for on-axis field) for the field behavior along the ***entire*** propagation path was found, leaving the theory without the major advantage of a standard theory of monochromatic Gaussian beams. The ability of theory to globally address the propagation, in particular, in between near- and far-field areas, is essential, since in practice, that intermediate area could be of most significance, with the diffraction distance for the highest spectral frequency, $z_d = r_0^2/ct_0$ (where $2t_0$ is a pulse time-width, and $2r_0$ a pulse transverse size), being considerably large. For $2t_0 \sim 400\ fs$ and $2r_0 \sim 1\ cm$ [3], one has $z_d \sim 40cm$, the same as e. g. for $2t_0 \sim 4\ fs$ and $2r_0 \sim 1\ mm$.

We derive here a simple equation for on-axis field (with a Gaussian initial spatial profile) valid for an ***arbitrary*** temporary profile and for any distance from the source. Using that equation, we obtain close-form solutions for the field transformation due to diffraction for some temporal profiles, in particular $\cosh^{-1}$-like and Gaussian profiles, and show that in far-field area pulses demonstrate time-derivative behavior regardless of their

frequency limit, we find a general solution valid for ***any*** spatia1 and temporal profiles of the field, which also explains in simple antenna terms the nature of time-derivative behavior; this solution is also valid in far-field area for ***any*** frequency.

Consider now a pulse propagating along the z axis and having an ***arbitrary*** time dependence and a known transverse profile, at the point $z = 0$. We assume at this point a high-frequency limit, meaning that the shortest temporal scale of the pulse, t_0 (in the extreme case of non-oscillating, half-cycle pulse, it is its initial half-timewidth, see below), and its respective longitudinal scale, ct_0, are much shorter than its transverse radius, r_0,

$$r_0 \gg ct_0, \quad or \quad z_d/r_0 \gg 1. \tag{10.1}$$

The frequency components of the largest part of its spectrum, $c/r_0 < \omega < t_0^{-1}$, will propagate with relatively small diffraction, so that one can apply a standard paraxial approximation (PA) to each one of them. Within PA, the diffraction of a monochromatic field, $E_\omega \exp[-i\omega(t - z/c)]$, in a free space, is described using a PA wave equation similar to a Schrödinger equation for a free electron:

$$-2i(\omega/c)\partial E_\omega/\partial z + \Delta_\perp E_\omega = 0, \tag{10.2}$$

where $\Delta_\perp$ is a transverse Laplacian; note that PA allows one to neglect polarization of the field and reduce the problem to a scalar one. We will also assume the field cylindrically symmetric in its cross-section, so that $\Delta_\perp = \partial^2/\partial r^2 + r^{-1}\,\partial/\partial r$, where r is the radial distance from the axis z in the cross-section. With the most of the available or to be available sources of HCPs, one can assume that the field at the source has a plane phase front for all the spectral components, so that their waists are located at the source. The spatially-Gaussian field at the source, $z=0$, can then be written as $E_0(t)\exp(-r^2/2r_0^2)$, where r_0 is the radius of the spatial field profile at the level $\exp(-1/2)$ of peak amplitude, E_0. Writing the solution of PA equation (10.2) as a Fourier transform:

$$E(\tilde{t}, r, z) = (2\pi)^{-1/2} \int_{-\infty}^{\infty} S(\omega, r, z) e^{i\omega\tilde{t}} d\omega \tag{10.3}$$

where $\tilde{t} = t - z/c$ is a retarded time, we have the field spectrum $S(\omega, r, z)$ for a Gaussian mode as:

$$S(\omega, r, z) = D(\omega, z) S_0(\omega) \exp[-(r^2/2r_0^2) D(\omega, z)], \tag{10.4}$$

Here $S_0(\omega) = (2\pi)^{-1/2} \int_{-\infty}^{\infty} E_0(t) \exp(-i\omega t) dt$ is the spectrum of original pulse, and

$$D(\omega, z) = (1 - izc/\omega r_0^2)^{-1} \tag{10.5}$$

is a diffraction factor due to PA. For the on-axis field, $r=0$, we have $S_{on}(\omega, z) = D(\omega, z) S_0(\omega)$. By substituting this into (10.3), and introducing a dimensionless retardation time, $\tau \equiv (t - z/c)/t_0$, and propagation distance, $\zeta \equiv z/z_d = zct_0/r_0^2$, we derive a simple equation for the temporal dynamics of an on-axis field at ***any*** point ζ:

$$\partial E_{on}/\partial\tau + \zeta E_{on} = \partial E_0(\tau)/\partial\tau. \tag{10.6}$$

If the full energy of the field at source is finite, the solution for the on-axis field is:

$$E_{on}(\tau, \zeta) = E_0(\tau) - \zeta e^{-\zeta\tau} \int_{-s(\zeta)\,\infty}^{\tau} e^{\zeta t} E_0(t) dt, \tag{10.7}$$

where $s(x) = -1$ if $x < 0$, and $s(x) = 1$ otherwise. One can see that, as expected, in a near-field area, $\zeta \ll 1$, the original temporal pulse profile is almost conserved, $E_{on} \approx E_0(\tau)$. The most interesting and universal (see below) pulse transformation occurs in far-field area, $\zeta \gg 1$. In this case, E_{on} can be expanded as

$$E_{on}(\tau, \zeta) = -\sum_{n=1}^{n=\infty} \frac{1}{(-\zeta)^n} \frac{\partial^n E_0(\tau)}{\partial\tau^n} \tag{10.8}$$

so that as $\zeta \to \infty$, the on-axis far-field replicates time derivative of the original pulse:

$$E_{on}(\tau,\zeta) \to \zeta^{-1}\partial E_0(\tau)/\partial\tau. \tag{10.9}$$

All of the results (10.6)-(10.9) are true for an ***arbitrary*** initial temporal profile, $E_0(\tau)$. In particular, any HCP is transformed in the far-field area into a single-cycle pulse.

Writing Eq. (10.6) in real time, $\partial E_{on}/\partial\tilde{t} + E_{on}/T = \partial E_0/\partial\tilde{t}$, where $T = r_0^2/cz$, we notice that it coincides with an equation for the voltage $U_R \propto E_{on}$ at a resistor R in a series RC circuit (high-pass filter) driven by a source $U_S \propto E_0(\tilde{t})$, so that the circuit relaxation time is $T=RC$. Since the only parameter with the dimensionality of resistance in a free-space propagation is the wave impedance of vacuum ($R = 120\,\pi$ ohm), the circuit capacitance is then $C \propto r_0^2/z$, which is consistent with a capacitor formed by electrodes having the pulse waist area $\propto r_0^2$ and spaced by z and thus provides an interesting and simple interpretation of the nature of pulse transformation in free space.

A simple example of the field evolution along the the entire path of propagation (i. e. for an arbitrary ζ), is given by a smooth bell-shaped initial profile $E_0(\tau) = \mathcal{E}_0(1+|\tau|)\exp(-|\tau|)$ with exponential tails at $|\tau| \to \infty$. Eq. (10.7) yields then:

$$\frac{E_{on}(\tau,\zeta)}{\mathcal{E}_0} = \frac{e^{-|\tau|}}{1-s(\tau)\zeta}\left[\frac{1}{1-s(\tau)\zeta} + |\tau|\right] + \frac{2\zeta e^{-\zeta\tau}[s(\zeta)+s(\tau)]}{(1-\zeta^2)^2}; \tag{10.10}$$

at $\zeta = 1$ and $\tau > 0$, the rhs of (10.10) is $exp(-\tau)(1-2\tau^2)/4$. A familiar profile $E_0 = \xi_0/\cosh(\tau)$ does not behave as nicely; in this case, a solution (10.7) in elementary functions exists if ζ is ***any rational*** number, but its form is different for different ζs. At $\zeta=1$, one has $E_{on}(\tau,1) = E_0(\tau) - \mathcal{E}_0 e^{-\tau}\ln(1+e^{2\tau})$.

The solution (10.7) for an Gaussian initial temporal profile $E_0(t) = \mathcal{E}_0 \exp(-t^2/2t_0^2) = \mathcal{E}_0 \exp(-\tau^2/2)$ (here t_0 is the pulse half-width at $exp(-1/2)$ peak amplitude), having the spectrum $S_0 = \mathcal{E}_0 t_0 \exp(-\omega^2 t_0^2/2)$, is handled analytically for ***any*** ζ:

$$E_{on}(\tau,\zeta) = E_0(\tau)\{1 - \zeta\sqrt{\pi/2}\,\exp[(\tau-\zeta)^2/2]\,[s(\zeta) + erf((\tau-\zeta)/\sqrt{2})]\} \tag{10.11}$$

where $erf(x) \equiv 2\pi^{-1/2}\int_0^x \exp(-x^2)dx$ [32]. As the pulse propagates, its total on-axis energy per unity area, $W_{on}(\zeta) = \int_{-\infty}^{\infty} |S_{on}(\omega,\zeta)|^2\, d\omega = \int_{-\infty}^{\infty} E^2(t,\zeta)dt$, decreases as:

$$w(\zeta) \equiv \frac{W_{on}(\zeta)}{W_{on}(0)} = 1 - \zeta\sqrt{\pi}\, e^{\zeta^2}[s(\zeta) - erf(\zeta)], \tag{10.12}$$

which in the limit $\zeta \to \infty$ yields $w(\zeta) \to (2\zeta^2)^{-1}$, as expected. The evolution of the profile and spectrum of the on-axis Gaussian HCP as it propagates away from the source, is shown in Fig. 9; one can clearly see that the pulse sheds off lower frequencies to finally form almost exact mimic of the time-derivative of the original Gaussian pulse. The zero point (i. e. the moment τ_z where $E = 0$), is moving closer to $\tau = 0$ as the distance $\zeta >> 1$ increases. Using first two terms in the expansion (10.8), with the zero point found from $\tau_z \partial E_/\partial\tau \approx \partial^2 E_/\partial\tau^2$, we have $\tau_z \approx \zeta^{-1}$.

The lower-frequency radiation diffracts stronger and hence is found mostly off-axis, where, by the same token, the higher frequencies are weaker. all of which results in the lengthening of the pulse. The smaller the diffraction angle at the cut-off frequency, $\theta_d = ct_0/r_0$ ($<<1$ due to (10. 1)), the stronger this effect is pronounced. In far-field area, $\zeta >> 1$, we introduce the angle of observation, $\theta = r/z$, and an angular factor due to diffraction, $\Theta = \sqrt{1+\theta^2/\theta_d^2}$, and approximate the spectrum (10.4) of the pulse as: $S_{off}(\omega,\theta,\zeta) \approx (i\omega t_0)\zeta^{-1} S_0(\omega)\exp[-(i\omega t_0 + \omega^2 t_0^2)(\theta^2/2\theta_d^2)]$, which in the case of Gaussian initial temporal profile, yields an off-axis pulse in far-filed area:

$$E_{off}(\tau,\theta,\zeta) \approx \left(\frac{\mathcal{E}_0}{\zeta\Theta}\right)\frac{\partial\{\exp[-(\tau-\tau_{sp})^2/2\Theta^2]\}}{\partial\tau} \tag{10.13}$$

(10.13) resembles (10.9) with the main difference being that off-axis pulse stretches in time by the factor Θ and its spectrum is respectively "squeezed" by the same factor.

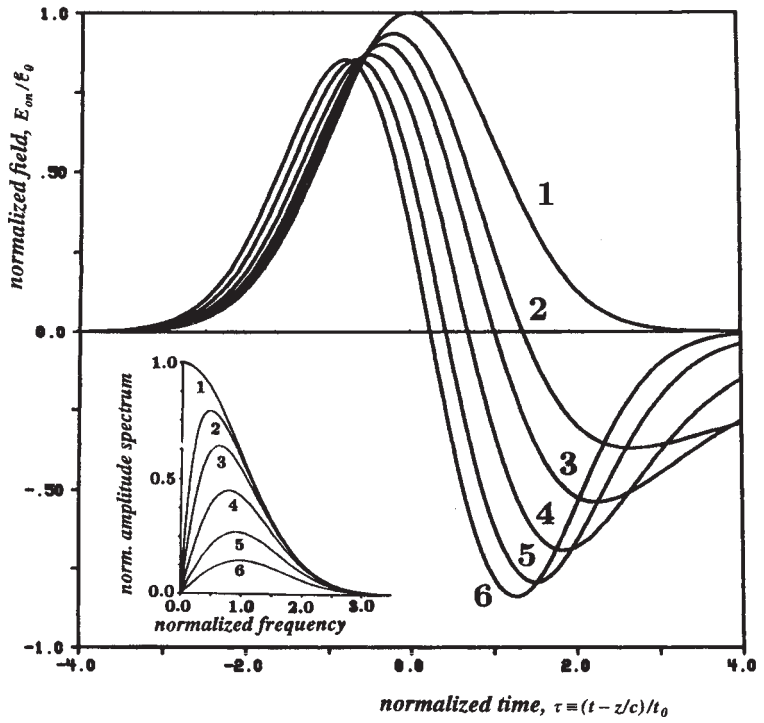

Fig. 9. The evolution of the on-axis temporal profile (normalized field, $E_{on}/\mathcal{E}_0$ *vs* normalized time, τ, and the normalized amplitude spectrum, $|S|/\mathcal{E}_0 t_0$, *vs* normalized frequency, $\nu \equiv \omega t_0$ (*inset*), of the initially Gaussian half-cycle pulse, as it propagates along the axis $\zeta = zct_0/r_0^2$. Curves: 1, $\zeta = 0$; 2, $\zeta = 0.25$; 3, $\zeta = 0.5$; 4, $\zeta = 1$; 5, $\zeta = 2$; 6, $\zeta = 4$. For the sake of comparison, each curve in the main Fig. is scaled up by the factor $w^{-1/2}(\zeta)$.

In the so called low-frequency limit $r_0 \ll ct_0$, opposite to (10.1), with the source size being much smaller that the wavelength $\lambda = 2\pi c/\omega$ of any frequency component, all the components have the same dependence on the angle of propagation; also, the initial spatial profile of the field becomes unimportant. The radiation pattern at each frequency is then determined by an elementary (i. e. point-like) dipole formed by the field distribution, $\vec{E}_0(t,x,y)$. At the distance $\rho = \sqrt{x^2+y^2+z^2} \gg r_0$ from this point-like source (i. e. away from the very small near-field area $\rho_{near} \ll \lambda$), and assuming that the field $\vec{E}_0$ is linearly polarized, the spectrum of ***radiative*** waves is:

$$S(\omega,\rho,\theta) = \frac{i\omega \cos\theta}{2\pi\rho c} \iint_{-\infty}^{\infty} S_0(\omega,x,y)dxdy, \qquad (10.14)$$

where θ is now the angle between the axis z and the direction of propagation, $\vec{u}_k$ ($|\vec{u}_k| = 1$), in the plane of the vector of polarization, $\vec{e}_0 = \vec{E}_0/E_0$, and the observation point.

The Fourier transform of (10.14) produces the same time-derivative profile everywhere,

$$\vec{E}(\tilde{t},\rho,\theta)=(\vec{e}_E/2\pi\rho c)\,[\partial q_0(\tilde{t})/\partial\tilde{t}],\quad q_0(t)=\int\!\!\int_{-\infty}^{\infty}E_0(t,x,y)dxdy \tag{10.15}$$

where $\vec{e}_E=\vec{u}_k\times[\vec{e}_0\times\vec{u}_k]$ is the polarization vector of radiative field, $|\vec{e}_E|=\cos\theta$. Eq. (10.15) explains pulse transformation in simple terms of elementary dipole antennae driven by a current $i_0(\tilde{t})=\partial q_0/\partial\tilde{t}$, which is induced by the dynamics of one of the dipole electrical "charges" q_0 originated by the source field, E_0; hence time-derivative temporal profile. Bearing in mind that for a Gaussian beam, $q_0=2\pi r_0^2\mathcal{E}_0$, Eq. (10.15) at $\theta=0$ is consistent with the Gaussian on-axis far-field (10.9), indicating that the results (10.6-10.12) for the ***on–axis*** field are valid regardless of the condition (10.1). Furthermore, in far-field area, Eq. (10.15) describes an on-axis field for ***any*** distribution, ***regardless*** of whether it is Gaussian or not.

The dispersion and transformation of the pulse due to the propagation and diffraction can to great degree be reversed. The feasibility of that is related to the time/space reciprocity manifested here by Eq. (10.6) being invariant to the simultaneous sign reversal of time τ and distance ζ. (The same is true for the solution (10.7), if $E_0(\tau)$ is a symmetric function, see Eqs. (10.10)-(10.12).) In practice, the diffracted HCP can be transformed back almost into its original temporal profile (except for its ***cw*** component) by reflecting its diffracted wave front e. g. from a spherical concave mirror, if the angular aperture of the mirror is significantly larger than the diffraction angle, θ_d. If such a mirror has the radius of curvature R_m and is situated sufficiently far from the source, with the distance between them being $f_1 >> z_d$, the pulse is focused again into a tight spot at the distance f_2, determined by a standard optical mirror formula, $f_1^{-1}+f_2^{-1}=2R_m^{-1}$. If $f_2<f_1$, the area of this spot is smaller that that of the original spot, and the amplitude of the focused pulse is larger by the factor f_1/f_2. The residual distortion of the pulse (in particular, slight bipolarity of initially unipolar HCP) will be due to lower-frequency diffraction losses at the mirror; the larger the mirror size, the smaller this effect. In the case of point-like source, pulse restoration can be achieved by using a full ellipsoid of revolution, with the source and observation points situated at the foci of the ellipsoid.

11. CONCLUSION

In conclusion, we have theoretically demonstrated feasibility of powerful, near- and sub-femtosecond sub-cycle EM pulses and solitary waves, EM bubbles, supported by both quantum and classical nonlinear media. We have shown how their maximum amplitude and minimum length are limited by the atomic ionization. It follows from our theory that ***10 – 0.1 fs*** EMBs can be generated by the available half-cycle pulses and short laser pulses; the peak EMB intensity can reach ~ $10^{14}-10^{16}$ W/cm^2. Those results represent only the very first steps in the exploration of the new time domain. Our hope is that EMBs will be experimentally observed in the near future. This will pose new set of problems, such as EMB detection and characterization, separation, gating, control, focusing and guiding, and exploring various EMB applications. In a transverse-limited EM field, a zero-frequency spectral component of the incident HCP will not propagate beyond the near-field area, and in the far-field area, EMB will assume a modified profile. Using analytic approach to the diffraction-induced transformation of pulses with arbitrary temporal profiles, including half-cycle pulses, we found close-form solutions for the propagation of most commonly used initial spatio-temporal profiles, and explained the nature of time-derivative transformation in far-field area for arbitrary pulses.

The new time domain, being largely an uncharted territory, holds a lot of promises for the physics of field-matter interaction. The most familiar nonlinear effects and parameters associated with coherent light-matter interactions (harmonic generation, self-induced transparency, photon echoes, soliton generation and propagation, saturation of all kinds, n_2 , $\chi^{(3)}$, etc.) are likely to take on entirely different forms, or may even cease to exist. One of the most fundamental and intriguing phenomenon is the field ionization of atoms, molecules, and semiconductor quantum wells by a super-short pulse with the amplitude comparable to or larger than the ionization threshold. Such pulses could cause a substantial "shake-up" excitation or ionization of an atomic system within the time much shorter than any characteristic time of the system. In our most recent research [33] we showed that a few ***fs*** long and ***unipolar*** EMB acting upon a semiconductor quantum well, can cause both ***forward*** and ***backward*** field ionization, with the photoelectrons emitted in ***both*** directions (i. e. not only in the direction of the ionizing unipolar field) with comparable intensities. Even more fundamental and exciting results are obtained for the hydrogen atom hit by a sub-cycle pulse with an sub-atomic unit amplitude. We also observed that the ionization response of the atom consists of a sequence of well-separated peaks resulting in strong spatio-temporal inhomogeneity of the photoelectron cloud, and found an explanation of such a behavior.

This work is supported by AFOSR. The work by SFS is in part supported by the Deutsche Forschungsgemeinschaft. AEK is a recipient of the Alexander von Humboldt Award for Senior US Scientists of AvH Foundation of Germany.

REFERENCES

1. S. L. McCall and E. L. Hahn, Phys. Rev. Lett. ***18,*** 908 (1967).
2. P. W. Smith, Proc. IEEE, 1342 (1970) and references therein.
3. A. Hasegava and F. D. Tappert, Appl. Phys. Lett. ***23,*** 142 (1971).
4. V. E. Zakharov and A. B. Shabat, Sov. Phys. JETP ***34,*** 62 (1972).
5. (a) R. L. Fork, C. H. Brito Cruz, P. C. Becker, and C. V. Shank, Opt. Lett., ***12,*** 483 (1987); (b) M. Nisoli, S. De Silvestri, O. Svelto, R. Szipócs, K. Ferencz, Ch. Spielmann, S. Sartania, and F. Krausz, Opt. Lett. ***22,*** 522 (1997).
6. K. E. Oughstun and H. Xiao, Phys. Rev. Lett. ***78,*** 642 (1997); K. E. Oughstun and G. C. Sherman, ***Electromagnetic pulse propagation in casual dielectrics*** (Springer, Berlin, 1994).
7. P. R. Smith, D. H. Auston, and M. S. Nuss, IEEE JQE, ***24,*** 255 (1988).
8. D. Grischkowsky, S. Keidin, M. van Exter, and Ch. Fattinger, JOSA B, ***7,*** 2006 (1990); R. A. Cheville and D. Grischkowsky, Opt. Lett. ***20,*** 1646 (1995).
9. J. H. Glownia, J. A. Misewich, and P. P. Sorokin, J. Chem. Phys. ***92,*** 3335 (1990);
10. B. B. Hu and M. S. Nuss, Opt. Lett. ***20,*** 1716 (1995);
11. R. R. Jones, D. You, and P. H. Bucksbaum, Phys. Rev. Lett. ***70,*** 1236 (1993); C. O. Reinhold, M. Melles, H. Shao, and J. Burgdorfer, J. Phys. B ***26,*** L659 (1993).
12. A. E. Kaplan, Phys. Rev. Lett. ***73,*** 1243 (1994); A. E. Kaplanand P. L. Shkolnikov, JOSA B ***13,*** 412 (1996).
13. A. E. Kaplan and P. L. Shkolnikov, Phys. Rev. Lett. ***75,*** 2316 (1995); also in Int. J. of Nonl. Opt. Phys. & Materials, ***4,*** 831 (1995).

14. A. E. Kaplan, S. F. Straub and P. L. Shkolnikov, Opt. Lett., ***22,*** 405 (1997); also to appear in JOSA B ***14*** (1997).

15. R. K. Bullough and F. Ahmad, Phys. Rev. Lett. ***27,*** 330 (1971); J. C. Eilbeck, J. D. Gibbon, P. J. Caudrey, and R. K. Bullough, J. Phys. A ***6,*** 1337 (1973).

16. E. M. Belenov, A. V. Nazarkin, and V. A. Ushchapovskii, Sov. Phys. JETP ***73,*** 423 (1991).

17. A. I. Maimistov, Opt. & Spectroscopy, ***76,*** 569 (1994) and ***78,*** 435 (1995).

18. B. Kohler, V. Yakovlev, J. Ghe, M. Messina, K. R. Wilson, N. Schwentner, R. M. Whitnell, and Y. Yan, Phys. Rev. Lett. ***74,*** 3360 (1995)

19. A. E. Kaplan and P. L. Shkolnikov, Phys.Rev. A. ***49,*** 1275 (1994).

20. For a harmonic oscillator with a frequency ω_0, it is natural to choose $U_0 = \hbar\omega_0$, with $x_0 = \sqrt{\lambda_C \lambda_0}$, where $\lambda_C = \hbar/m_e c = 2.4 \times 10^{-2} \text{Å}$ is the Compton wavelength.

21. If nonlinearity is negative, $a < 0$, one can expect formation of "dark" EMB (a solitary "hole" propagating on a ***cw*** field background): $f(\tau) \propto f_0 \tanh(\tau f_0)$, $f_0 = const.$

22. D. G. Lappas, M. V. Fedorov, and J. H. Eberly, Phys. Rev. ***A 47,*** 1327 (1993); J. H. Eberly, Q. Su, and J. Javanainen, JOSA B ***6,*** 1289 (1989).

23. Recent studies of shock-like ***envelope*** fronts can be found, e. g. in S. R. Hartmann and J. T. Massanah, Opt. Lett. ***16,*** 1349 (1991); E. Hudis and A. E. Kaplan, Opt. Lett. ***19,*** 616 (1994); W. Forysiak, R. G. Flesh, J. V. Moloney, and E. M. Wright, Phys. Rev. Lett. ***76,*** 3695 (1996).

24. R. M. Miura, J. of Math. Physics, ***9,*** 1202 (1968); R. M. Miura , C. S. Gardner and M. D. Kruskal, ***ibid,*** 1204 (1968); M. Wadati, J. Phys. Soc. Japan, ***32,*** 1681 (1972); ***ibid, 34,*** 1289 (1973)

25. L. Xu, D. H. Auston, and A. Hasegava, Phys. Rev. ***A45,*** 3184 (1992).

26. A. McPherson, G. Gibson, H. Jara, U. Johann, T. S. Luk, I. A. McIntyre, K. Boyer, and C. K. Rhodes, JOSA B ***4,*** 595 (1987); M. Ferray, A. L'Huillier, X. F. Li, L. A. Lompre, G. Mainfray, and C. Manus, J. Phys. B ***21,*** L31 (1988); A. L'Huillier and Ph. Balcou, Phys. Rev. Lett. ***70,*** 774 (1993); L'Huillier, A, Lompre, L. A., Mainfray, G., and Manus, C., in *Atoms Intense Laser Field* , Ed. M. Gavrila (Acad. Press, Inc., Boston, 1992), p. 139-206.

27. A. E. Kaplan, to appear in JOSA B.

28. Max Born and Emil Wolf, ***Principles of Optics,*** 6-th edition (Pergamon Press, NY, 1980).

29. A. Siegman, ***Lasers*** (Univ. Science, Mill Valley, CA, 1986); A. Yariv, ***Quantum Electronics*** (Wiley, NY, 1989).

30. M. van Exeter and D. R. Grischkowsky, IEEE Trans. Microwave Theory Techn., ***38,*** 1684 (1990); J. Bromage, S. Radic, G. P. Agrawal, C. R. Stroud, Jr., P. M. Fauchet, and R. Sobolevski, Opt. Lett. ***22,*** 627 (1997).

31. R. W. Ziolkowski and J. B. Judkins, JOSA B ***9,*** 2021 (1992).

32. I. S. Gradshtein and I. M. Ryzhik, ***Tables of Integrals, Series, and Products*** (Academic, NY, 1980).

33. A. E. Kaplan, S. F. Straub and P. L. Shkolnikov, to be published; first reported in Quant. Electr. & Laser Science Conf., v. 12, 1997 OSA Techn. Digest Series (OSA, Washington, DC, 1997), p. 31.